

Article

Analysis, Control and Optimal Placement of Static Synchronous Compensator with/without Battery Energy Storage

Ganggang Tu ^{1,*}  and Yanjun Li ²  and Ji Xiang ¹ ¹ College of Electrical Engineering, Zhejiang University, Hangzhou 310027, China; jxiang@zju.edu.cn² School of Information and Electrical Engineering, Zhejiang University City College, Hangzhou 310015, China; liyanjun@zucc.edu.cn

* Correspondence: tuganggang@zju.edu.cn

Received: 12 November 2019; Accepted: 5 December 2019; Published: 10 December 2019



Abstract: Static synchronous compensator (STATCOM) and battery energy storage (BES) have been increasingly employed in power systems for the reliable and economic operation of power transmission. However, the transient interaction between the electrical power of synchronous generator (SG) and the active power of STATCOM with/without BES is still misunderstood and treated incorrectly. This paper presents an analysis of this interaction and investigates the control and optimal placement of STATCOM with/without BES for the purpose of improving SG's damping, and thus enhancing system's oscillation damping performance. The results show that (1) the deviated electrical power of SG is not equal to the active power of STATCOM. Instead, it is related to STATCOM's current, placement and SG's electrical states, (2) with the increased damping as the index, the optimal location for STATCOM with BES is at the terminal of SG, while it is at the electrical mid-point of the transmission line for STATCOM without BES. Non-linear simulations and eigenvalue analysis are performed to validate the correctness of the above results.

Keywords: battery energy storage; transient analysis; oscillation damping; optimal placement

1. Introduction

The stability of power system has been a key concern for secure system operation [1]. Electromechanical oscillations can happen when subject to the random contingencies, such as line faults, switching of loads or outage of transformers or generators. The poorly-damped or unstable oscillations can cause large-scale power system blackouts [2], such as the blackout of 14 August 2003 in North America [3]. Therefore, installing additional devices or developing control methods to damp out the oscillations is of considerable practical interest.

1.1. Literature Review

To improve system's damping, different kinds of power system stabilizers (PSSs) are designed, such as multi-objective PSS [4], wavelet-based PSS [5] and distributed PSS [6]. In principle, the PSSs inject an additional damping signal to enhance the oscillation damping performance by controlling the excitation voltage of the synchronous generator (SG). Renewable energy has also been investigated to mitigate power system oscillations. For instance, in [7], the authors presented an optimized power point tracking controller which shifts the wind turbine (WT) from maximum power point tracking to provide oscillation damping to the grid. In [8], the authors proposed a novel approach to coordinate the aggregated output power of offshore wind farm and its onshore voltage source converter for effective power oscillation damping. In [9], the authors proposed a damping strategy

for large-scale photovoltaic (PV) plants using multiple-model adaptive control. In [10], the authors proposed a composite strategy for PV plants to achieve both frequency response and oscillation damping. Another option of increasing the system damping is through regulating the reactive power or the reactance of the flexible alternating current transmission system (FACTS) devices, including thyristor controlled series compensation (TCSC) [11], static VAR compensator (SVC) [12], and static synchronous compensator (STATCOM) [13,14].

STATCOM is a shunt compensation device, which introduces voltage-source converter to achieve advanced power control. In practical applications, STATCOM has several advantages over other FACTS devices such as size, weight, and cost reduction, precise and continuous reactive power control with fast response. Therefore, many research activities about STATCOM to improve power system stability have been reported. Conventionally, STATCOM is used for voltage regulation in transmission lines through proportional-integral (PI) control. To improve the dynamic performance of PI control, particle swarm optimization (PSO) has been adopted to adjust the controller gains [15]. Other control strategies, such as pole-placement and linear quadratic regulator [16], are also reported. Damping controllers based on STATCOM have also been investigated in the literature. In this field, the STATCOM-based dampers act an supplementary controller and the ancillary damping signal is superimposed on the reference of the AC bus voltage control [13] or the DC bus voltage control [17]. In the design of STATCOM-based damper, the authors in [14] formulated it as an optimization problem and the real-coded genetic algorithm is adopted to search for the optimal parameter settings. Comparison between a STATCOM-based damping controller and PSS and SVC is also investigated in [18].

In recent years, battery energy storage (BES) techniques are fast developing due to the advancement of power electronics and battery technology. This leads to their increasing applications in power systems for different objectives. For example, In [19], the BES is used to follow the load demands as well as achieve economic operation. In the field of renewable generation, BES has also been investigated to smooth the power output of wind power [20] and PV power [21]. In the operation of microgrid, the BES is coordinated with the distributed renewable energy in a decentralized manner to reduce both the frequency and voltage deviations after severe disturbances [22]. Since the integration of BES into STATCOM enables itself fast active power provision capability, various control strategies have been proposed to improve the stability of power systems. For example, in [23], a distributed control framework based on parametric feedback linearization is proposed to cancel out the nonlinear dynamics among generators and balance the swing equation after disturbances. In [24], a consensus-based controller is presented to maintain the synchronism between neighboring SGs when subject to a fault. In [25], a linear feedback optimal controller is designed relying on timely system-wide state information. In [26], a distributed control considering the communication delay and cyber-physical disturbances is presented. In [27], the authors further considered the impact of false data injection attacks in the distributed control of BES. In [28], a model predictive controller is presented to deal with model uncertainties and sensor measurement noise. In [29], a multiagent framework is proposed to address the limited capacity and availability of BES, and the absence and delay of sensor measurements. However, in these papers [23–29], the authors developed the control method of STATCOM with BES based on an incorrect model, which simply assumes that the active power of STATCOM with BES is fully added into SG's electrical power of the swing equation. This assumption is inconsistent with the actual interaction between BES and SG, and thus limit the performance of BES in enhancing the system stability.

1.2. Contributions

In this paper, we provide a comprehensive analysis of both STATCOM with and without BES on the transient electrical power of SG. Meanwhile, the control and optimal placement are investigated to improve SG's damping considering the dynamical interactions between SG and STATCOM. For the analysis of STATCOM on SG's dynamics, the single machine infinite bus system is adopted

since it has been widely used in power system dynamics studies. It is shown that the deviated electrical power of SG is not equal to the active power of STATCOM. Instead, it is related to both the placement of STATCOM and the electrical states of SG, and is linear to the active and reactive current of STATCOM. Based on this result, a damping control strategy of regulating STATCOM's current is proposed in order to improve SG's damping and thus improve the system's oscillation damping performance. Optimal placement of STATCOM with/without BES is also investigated to maximum increase system damping, which is different from conventional researches where the placement is optimized to minimize the power system loss, enhance voltage quality and stability or reduce device size of STATCOM [30]. The main results of this paper are the following:

1. Transiently, the installment of STATCOM will deviate the electrical power of SG. The deviated value is not equal to the active power of STATCOM. Instead, it is related to STATCOM's current, placement and SG's electrical states. However, in many previous researches, such as [23–29], the authors developed the control method by simply assuming that the active power of STATCOM with BES is fully added into SG's electrical power.
2. To maximally increase the system damping, the optimal placement for STATCOM with BES is at the terminal of SG. While for STATCOM without BES, it is at the electrical mid-point of the transmission line, which is consistent with the optimal location of conventional mid-point voltage regulation of STATCOM without BES [30].

1.3. Organization

The structure of this paper is organized as follows. Section 2 describes the mathematical model for SG and STATCOM with/without BES. Section 3 investigates the dynamical interactions between STATCOM and SG. Section 4 develops the proposed damping control strategy for improving SG's damping. Section 5 investigates the optimal location for both STATCOM with and without BES. Section 6 verifies previous analytical results. Conclusions are drawn in Section 7.

2. System Model

In this section, the considered SG and STATCOM model are briefly presented for the transient analysis of STATCOM with/without BES on SG's dynamics.

2.1. SG Model

According to [31], the dynamics of SG is represented by the following swing equations:

$$\begin{aligned}\dot{\delta} &= w - w_0 \\ \dot{w} &= -\frac{D}{2H}(w - w_0) + \frac{w_0}{2H}(P_m - P_e).\end{aligned}\quad (1)$$

Here, δ is the rotor angle; w is the rotor speed; w_0 is the rated rotor speed; H is the moment of inertia; D is the damping coefficient of SG; P_m is the mechanical power, and it is regulated by the turbine governor to meet the system load requirements; P_e is the electrical power that is generated by SG. Here, we note that, P_e is determined by the electrical interactions among SGs and the other system devices. In detail, P_e is calculated from the electrical states of the node in the power network, i.e., the voltage magnitude, power angle and the power frequency etc. Using this mechanism, the widely-used PSS injects a stabilizing signal into P_e through the excitation circuit of SG [32]. Similarly, the electrical power of SG can also be influenced by regulating STATCOM's electrical states, such as the active or reactive power, the active or reactive current. Differing from P_e , the mechanical power P_m is directly controlled by the turbine governor [33]. In the transient studies of power system, P_m is usually regarded as the steady state value due to its slow variation compared to the electromechanical oscillations.

2.2. STATCOM with/without BES Model

In this paper, we consider both STATCOM with and without BES for SG's damping improvement. The STATCOM without BES is a shunt-connected device, which can only provide controllable reactive power from lagging to leading [34]. The capacitor or reactor are not employed to generate reactive power. Instead, they are installed to keep a constant DC voltage for the operation of the voltage-source converter (VSC). Through integrating a BES into the capacitor bank (STATCOM with BES), the STATCOM enables itself active power provision ability and thus more capability and flexibility of improving SG's dynamics.

The diagram of STATCOM with/without BES is shown in Figure 1. The VSC is a DC/AC converter, which simultaneously controls the active and reactive power of STATCOM that is delivered to the power grid. The VSC is usually operating in current-mode control by directly regulating the AC side current for the purpose of overload protection, parameter robustness and dynamic performance [35]. Hence, in the transient study of power system, STATCOMs can be represented by an ideal controllable current source $I_s = I_{ds} + jI_{qs}$, shown in Figure 1 [36]. According to [37], by properly designing the VSC current controller, the closed-loop function of $I_{ds}(s)$ and $I_{qs}(s)$ are

$$\begin{aligned}\frac{I_{ds}(s)}{I_{dsref}(s)} &= \frac{1}{\tau s + 1}, \\ \frac{I_{qs}(s)}{I_{qsref}(s)} &= \frac{1}{\tau s + 1}.\end{aligned}\quad (2)$$

Here, $I_{dsref}(s)$ and $I_{qsref}(s)$ are the d-axis and q-axis reference current respectively, which are calculated by the upper control of STATCOM according to its specific application; τ is a time constant and is a design choice. In practice, τ should be made small for a fast current-control response but adequately large such that $\frac{1}{\tau}$ is adequately smaller than the switching frequency of the VSC. Depending on the specific application and the switching frequency of VSC, τ is typically chosen from 0.5–5 ms [37].

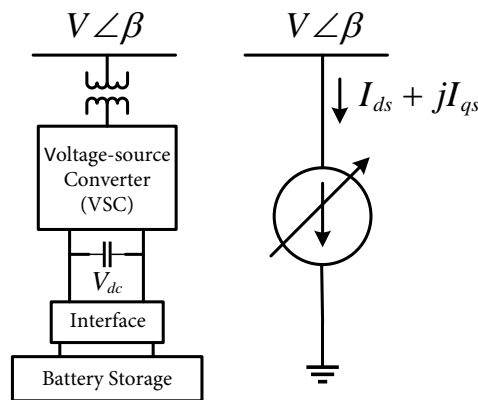


Figure 1. Static synchronous compensator (STATCOM) with/without battery energy storage (BES).

3. Transient Analysis

In this section, the single machine infinite bus (SMIB) system is adopted to analyze the transient interactions between STATCOM and SG's electrical power. The second order model of SMIB system is able to capture the dynamical characteristics and behaviors of power systems. Therefore, it has been widely used in the analysis and control of electromechanical oscillations [32,33,38]. As shown in Figure 2, the SMIB system is composed of a SG and an infinite bus, which are connected through a transmission line. The infinite bus has constant voltage magnitude and angle. The STATCOM is employed in the transmission line to investigate the transient interactions between STATCOM and SG.

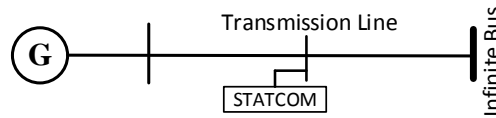


Figure 2. The single machine infinite bus (SMIB) with STATCOM deployed at the transmission line.

By representing SG with the classical model [33], neglecting the resistance of SG and transmission line, and using the STATCOM model in Figure 1, the system representation of Figure 2 is as shown in Figure 3a. Here, the terminal voltage of infinite bus is set as the reference phasor; E'_q is the quadrature-axis transient voltage of SG; X'_d is the d -axis transient synchronous reactance of SG; X_{T1} and X_{T2} are the reactance of the transmission line, X_T is the total reactance of the transmission line and $X_{T1} + X_{T2} = X_T$; P and Q are the absorbed active and reactive power of STATCOM respectively.

In order to analyze the transient interactions between SG and STATCOM, we set the terminal voltage of STATCOM as reference phasor, that is, the terminal voltage angle of STATCOM is zero. Then, as shown in Figure 3b, the voltage of STATCOM becomes $V \angle 0$, the current of STATCOM becomes $I = I_d + jI_q$, the quadrature-axis transient voltage of SG becomes $E'_q \angle_{\delta-\beta}$, and the voltage of infinite bus becomes $E_B \angle_{-\beta}$. Through this treatment, the transient interactions between STATCOM and SG are analyzed.

The influence introduced by STATCOM, i.e., $I_d + jI_q$, on P_e can be formulated based on Figure 3b. Intuitively, the active and reactive power of STATCOM are

$$\begin{aligned} P &= V \cdot I_d, \\ Q &= -V \cdot I_q. \end{aligned} \quad (3)$$

This shows that the active and reactive power of STATCOM are decoupled, and are determined by its d -axis (I_d) and q -axis (I_q) current respectively. In the following of this paper, for the ease of understanding, I_d and I_q are also called as active and reactive current respectively. Using the superposition theorem, the electrical power of SG is

$$P_e = \text{Real} \left\{ (E'_q \angle_{\delta-\beta}) \cdot (I_{e0} + \Delta I_e)^* \right\} \quad (4)$$

where

$$\begin{aligned} I_{e0} &= \frac{E'_q \angle_{\delta-\beta} - E_B \angle_{-\beta}}{(X'_d + X_T) \angle_{\pi/2}} \\ \Delta I_e &= \frac{X_{T2} (I_d + jI_q)}{X'_d + X_{T1} + X_{T2}} = \frac{X_{T2} (I_d + jI_q)}{X'_d + X_T}. \end{aligned} \quad (5)$$

Here, I_{e0} is the original current of SG when there is no STATCOM employed and ΔI_e is the deviation of SG's current caused by the deployment of STATCOM. Then,

$$P_e = P_{e0} + \Delta P_e \quad (6)$$

where

$$P_{e0} = \frac{E'_q E_B \sin \delta}{X_T + X'_d}, \quad (7)$$

$$\Delta P_e = \frac{X_{T2} E'_q}{X'_d + X_T} (\cos(\delta - \beta) I_d + \sin(\delta - \beta) I_q). \quad (8)$$

Here, P_{e0} is the original electrical power of SG when no STATCOM is installed and ΔP_e is the deviated power due to the installment of STATCOM. ΔP_e in Equation (8) finally shows the transient influence of STATCOM on the electrical power of SG. Due to the placement of STATCOM, the whole system's circuit model is added with a current source. As a result, this current source makes

the electrical power of SG deviate from its original value P_{e0} and become $P_{e0} + \Delta P_e$. The deviated value ΔP_e is related to both the placement of STATCOM (i.e., X_{T2}) and the electrical states of SG (i.e., E'_q). ΔP_e is also related to STATCOM's both active and reactive current (i.e., I_d, I_q), which are related to the active and reactive power of STATCOM respectively.

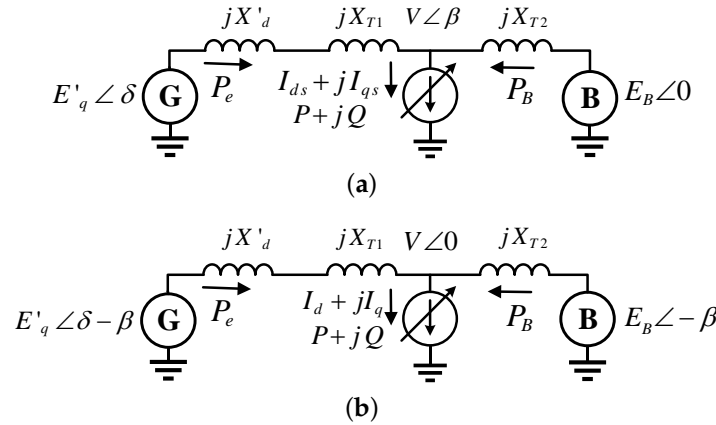


Figure 3. Circuit model of SMIB with STATCOM. (a) The terminal voltage of infinite bus as reference phasor. (b) The terminal voltage of STATCOM as reference phasor.

Accordingly, define I_{B0} is the original current of infinite bus when no STATCOM is installed, ΔI_B is the current deviation of the infinite bus caused by the installment of STATCOM, P_B is the delivered active power of infinite bus, P_{B0} is the electrical power of infinite bus without the deployment of STATCOM, ΔP_B is the deviation of the delivered active power of infinite bus introduced by STATCOM. Then,

$$\begin{aligned} P_B &= \text{Real} \{ (E_B \angle -\beta) \cdot (I_{B0} + \Delta I_B)^* \} \\ &= P_{B0} + \Delta P_B = -P_{e0} + \Delta P_B \\ \Delta P_B &= \frac{X'_d + X_{T1}}{X'_d + X_T} \cdot E_B (\cos \beta \cdot I_d - \sin \beta \cdot I_q). \end{aligned} \quad (9)$$

According to active power balance of this system, the active power of STATCOM can be computed by

$$P = P_e + P_B = \Delta P_e + \Delta P_B. \quad (10)$$

Equation (10) indicates that ΔP_e is not equal to P because $\Delta P_B \neq 0$ according to (9). The active power absorbed by STATCOM is only partially added onto the electrical power of SG, and the remaining part of the active power of STATCOM is added onto the infinite bus. However, in many previous researches, such as [23–29], the authors simply assume that it is fully added into SG. In detail, in the modeling process of SG with BES, the authors in [23–29] assumed that $\Delta P_e = P$, and the active power of STATCOM is fully added onto the dynamics of rotor speed. Then, the authors developed their control method based on this incorrect SG model. In fact, when a STATCOM with/without BES is installed, the SG model should still be as shown in (1). The only difference is that the placement of STATCOM will deviate the electrical power of SG during transient situations, and the deviated value is not equal to the active power of STATCOM according to (10), i.e., $\Delta P_e \neq P$. Moreover, according to (8), when there is only reactive power provided by STATCOM, i.e., $I_d = 0, P = 0, I_q \neq 0$, ΔP_e is not zero as well. This shows that STATCOM without BES is also capable of modulating the dynamics of SG, and also proves that the assumption of $\Delta P_e = P$ in [23–29] is incorrect.

4. Damping Control of STATCOM with/without BES

According to previous analysis, both STATCOM with and without BES are capable of influencing the electrical power of SG, and the deviated value (ΔP_e) is determined by STATCOM's active and reactive current. Based on this, a current-based damping control strategy is presented for STATCOM with and/or without BES to increase SG's damping and thus enhance system's oscillation damping performance.

4.1. Reference Current of STATCOM with BES

For STATCOM with BES, the reference current are controlled as

$$\begin{aligned} I_{dref} &= k_d(w - w_0) \frac{sT_w}{1 + sT_w}, \\ I_{qref} &= 0. \end{aligned} \quad (11)$$

Here, I_{dref} is set as proportional to the rotor speed deviation to increase the damping of SG. The washout block $\frac{sT_w}{1+sT_w}$ is a high-pass filter, which blocks the slow changes in the rotor speed at normal operational situations. By adding it, the control of STATCOM only works under abnormal situations such as a short-circuit fault at the transmission line. The reason of setting I_{qref} as zero is as follows. According to (8), ΔP_e of SG is related to both I_d and I_q of STATCOM. In practice, δ is normally slightly greater than β . Thus, $\cos(\delta - \beta)$ is much greater than $\sin(\delta - \beta)$. This means that the influence of I_d on ΔP_e is much larger than that of I_q . Meanwhile, in practice, the current of STATCOM should be kept below a certain value to ensure safe operation. Therefore, controlling I_{dref} to increase SG's damping is preferred for STATCOM with BES. As a result, I_{qref} here is controlled as zero for the purpose of efficiently utilizing the current capacity to increase the damping of SG.

4.2. Reference Current of STATCOM without BES

Similarly, the reference current of STATCOM without BES are controlled as

$$\begin{aligned} I_{dref} &= 0, \\ I_{qref} &= k_q(w - w_0) \frac{sT_w}{1 + sT_w}. \end{aligned} \quad (12)$$

Here, I_{dref} is set to be zero because STATCOM without BES has no active power provision ability. I_{qref} is set to improve SG's damping. The washout block $\frac{sT_w}{1+sT_w}$ is added to block the slow changes in the rotor speed at normal operational situations.

4.3. Damping Control Strategy of STATCOM with/without BES

The detailed damping control strategy for STATCOM with and/or without BES are shown in Figure 4. Here, it should be mentioned that the d-axis and q-axis are constructed by using the terminal voltage of STATCOM as reference phasor. The controlled I_{dref} and I_{qref} acts as an ancillary signal, which is added onto the current control loop. In the conventional damping controllers, the damping signal are usually added onto the AC or DC bus voltage control loop [13,14,17,18] or the active power control loop [39,40], which are an outer loop nested outside the current control loop. This means that the proposed damping control strategy should have a faster response when the disturbance is occurring.

The power reference P_{ref} and Q_{ref} are determined by the specific application of STATCOM. In particular, Q_{ref} could be adjusted to control the AC bus voltage. For STATCOM with BES, P_{ref} could be set to provide primary frequency response. For STATCOM without BES, P_{ref} could be set as zero, or adjusted to maintain a constant DC bus voltage for the VSC operation if the power losses are

considered. In the damping controller design, the limiter is to avoid the damage of STATCOM, and it is determined by STATCOM's power ratings. For STATCOM with BES, we assume that the allowable state of charge (SOC) of BES is ranging from SOC_{min} to SOC_{max} , and thus the current reference are controlled as

$$I_{dref} = \begin{cases} k_d(w - w_0) \frac{sT_w}{1+sT_w} & , SOC < SOC_{max}, w > w_0 \\ k_d(w - w_0) \frac{sT_w}{1+sT_w} & , SOC > SOC_{min}, w < w_0 \\ 0 & , \text{otherwise} \end{cases} \quad (13)$$

$$I_{qref} = 0.$$

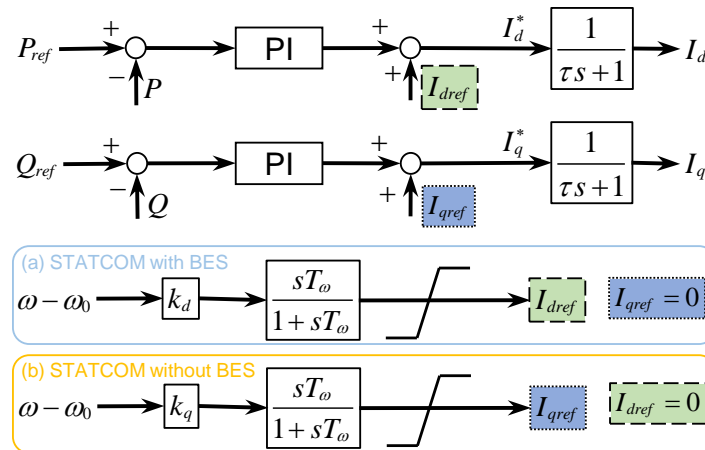


Figure 4. Damping control strategy of STATCOM: (a) With BES; (b) Without BES.

5. Optimal Placement of STATCOM with/without BES

According to (8), the location of STATCOM also influences the deviated electrical power of SG introduced by STATCOM. Therefore, the location of STATCOM with/without BES is here investigated in order to efficiently utilize STATCOM to increase the system damping and thus increase system oscillation damping performance. Here, the increased damping by STATCOM is selected as the measure for different placement of STATCOM. We note that this choice is different from conventional researches where the optimization goal is to minimize the power system loss, improve voltage quality and stability, or reduce the device size of STATCOM [30].

5.1. Optimal Placement of STATCOM with BES

Normally, the frequency of electromechanical oscillations is ranging from 0.1 to 2.0 Hz [41]. Therefore, the dynamics of STATCOM's current control, i.e., $\frac{1}{\tau s+1}$, can be approximated by a unity gain as τ is much smaller than the oscillation frequency. Meanwhile, the washout block can be also regarded as a unity gain. Then, ΔP_e in (8) of STATCOM with BES under the damping control strategy shown in Figure 4 becomes

$$\Delta P_e = \frac{X_{T2} E_q'}{X_d' + X_T} k_d \cos(\delta - \beta) (w - w_0). \quad (14)$$

Taking (14) and (8) into the SG model (1), we get the whole system model, shown below.

$$\begin{aligned} \dot{\delta} &= w - w_0 \\ \dot{w} &= -\frac{D + D_d}{2H} (w - w_0) + \frac{w_0}{2H} \left(P_m - \frac{E_q' E_B \sin \delta}{X_T + X_d'} \right), \end{aligned} \quad (15)$$

$$D_d = \frac{w_0 X_{T2} E'_q}{X'_d + X_T} k_d \cos(\delta - \beta). \quad (16)$$

Equation (16) shows that by regulating the current of STATCOM with BES according to Figure 4, the SG's damping is increased by D_d .

We now analyze the influence of D_d on the stability of the whole system. With initial operating condition represented by $\delta = \delta_0, w = w_0, \beta = \beta_0$ and assuming the mechanical power of SG is constant, the linearized model of (15) is

$$\begin{aligned} \Delta \dot{\delta} &= \Delta w \\ \Delta \dot{w} &= \frac{1}{2H} \left(-K_S \Delta \delta - K_D \Delta w \right) \end{aligned} \quad (17)$$

where

$$\begin{aligned} K_S &= \frac{w_0 E'_q E_B \cos \delta_0}{X_T + X'_d} \\ K_D &= D + D_{d0}, D_{d0} = \frac{w_0 X_{T2} E'_q}{X'_d + X_T} k_d \cos(\delta_0 - \beta_0). \end{aligned} \quad (18)$$

Note that system (17) is a second-order linear system and its natural frequency w_n and damping ratio ξ are

$$\begin{aligned} w_n &= \sqrt{\frac{K_S}{2H}}, \\ \xi &= \frac{K_D}{2\sqrt{2HK_S}}. \end{aligned} \quad (19)$$

We notice that the proposed control only changes the value of K_D according to (18). Then, the increased system damping ratio $\Delta \xi_d$ under proposed control is

$$\Delta \xi_d = \frac{D_{d0}}{2\sqrt{2HK_S}} = \frac{1}{2\sqrt{2HK_S}} \frac{w_0 X_{T2} E'_q}{X'_d + X_T} k_d \cos(\delta_0 - \beta_0). \quad (20)$$

According to Figure 3a, different placement of STATCOM corresponds to different X_{T2} and β_0 . X_{T2} increases monotonically with β_0 . In (20), $\delta_0 > \beta_0 > 0$. Thus, $\Delta \xi_d$ in (20) increases monotonically with both X_{T2} and β_0 . Therefore, the optimal placement for STATCOM with BES is at the terminal of SG such that β_0 and X_{T2} are the largest. By doing so, the improved damping $\Delta \xi_d$ increases to $\Delta \xi_{dmax}$, shown below.

$$\Delta \xi_{dmax} = \frac{1}{2\sqrt{2HK_S}} \frac{w_0 X_T E'_q}{X'_d + X_T} k_d \cos(\delta_0 - \beta_0). \quad (21)$$

When STATCOM with BES is employed at the terminal of SG, δ_0 becomes very close to β_0 . Thus, $\cos(\delta_0 - \beta_0)$ is reasonable to be approximated as $\cos(\delta_0 - \beta_0) \approx 1$ and

$$\Delta \xi_{dmax} = \frac{1}{2\sqrt{2HK_S}} \frac{w_0 X_T E'_q}{X'_d + X_T} k_d. \quad (22)$$

5.2. Optimal Placement of STATCOM without BES

The optimal placement of STATCOM without BES under the control in Figure 4 can be obtained following the similar treatment. The SG's deviated active power ΔP_e is

$$\Delta P_e = \frac{X_{T2} E'_q}{X'_d + X_T} k_q \sin(\delta - \beta)(w - w_0). \quad (23)$$

The whole system model becomes

$$\begin{aligned}\dot{\delta} &= w - w_0 \\ \dot{w} &= -\frac{D + D_q}{2H}(w - w_0) + \frac{w_0}{2H} \left(P_m - \frac{E'_q E_B \sin \delta}{X_T + X'_d} \right),\end{aligned}\quad (24)$$

$$D_q = \frac{w_0 X_{T2} E'_q}{X'_d + X_T} k_q \sin(\delta - \beta). \quad (25)$$

Here, D_q is the increased damping by STATCOM without BES. Comparing (24) with (15), the influence of D_q on the system stability can be analyzed with same pattern. After linearizing (24), the increased system damping ratio by STATCOM without BES $\Delta \xi_q$ is obtained, shown below.

$$\Delta \xi_q = \frac{D_{q0}}{2\sqrt{2HK_S}} = \frac{1}{2\sqrt{2HK_S}} \frac{w_0 X_{T2} E'_q}{X'_d + X_T} k_q \sin(\delta_0 - \beta_0). \quad (26)$$

Here, $\Delta \xi_q$ increases monotonically with X_{T2} , while decrease monotonically with β_0 . Thus, the optimal placement of STATCOM without BES is not the same as that of STATCOM with BES. Its optimal placement is now obtained by formulating the relationship between X_{T2} and β_0 .

According to Figure 3b,

$$\begin{aligned}P_e &= \frac{E'_q V \sin(\delta_0 - \beta_0)}{X'_d + X_T - X_{T2}} \\ P_B &= -\frac{E_B V \sin \beta_0}{X_{T2}} \\ P &= VI_d = P_e + P_B.\end{aligned}\quad (27)$$

Then, we get

$$\frac{E'_q \sin(\delta_0 - \beta_0)}{X'_d + X_T - X_{T2}} - \frac{E_B \sin \beta_0}{X_{T2}} = I_d. \quad (28)$$

As for STATCOM without BES, $I_d = 0$. Then, the relationship between X_{T2} and β_0 is

$$X_{T2} = \frac{(X'_d + X_T) E_B \sin \beta_0}{E'_q \sin(\delta_0 - \beta_0) + E_B \sin \beta_0}. \quad (29)$$

Substituting for X_{T2} from (29) in (25), we obtain

$$\Delta \xi_q = \frac{1}{2\sqrt{2HK_S}} w_0 k_q \frac{E'_q \sin(\delta_0 - \beta_0) \times E_B \sin \beta_0}{E'_q \sin(\delta_0 - \beta_0) + E_B \sin \beta_0}. \quad (30)$$

Then, after some calculation, $\Delta \xi_q$ is maximum at $\beta_0 = \beta_{opt}$ where

$$\frac{\cos \beta_{opt}}{E_B \sin^2 \beta_{opt}} = \frac{\cos(\delta_0 - \beta_{opt})}{E'_q \sin^2(\delta_0 - \beta_{opt})}. \quad (31)$$

Taking (31) into (29), we get the optimal $X_{T2,opt}$, which is

$$X_{T2,opt} = (X'_d + X_T) \frac{1}{1 + \sqrt{\frac{\cos(\delta_0 - \beta_{opt})}{\cos \beta_{opt}}}}. \quad (32)$$

Roughly, $E'_q \approx E_B$, then

$$\beta_{opt} \approx \frac{1}{2}\delta, \quad X_{T2,opt} \approx \frac{1}{2}(X'_d + X_T). \quad (33)$$

Then, taking $\beta_0 = \beta_{opt} \approx \frac{1}{2}\delta_0$ into (30), we get the maximum $\Delta\zeta_{qmax}$, shown below.

$$\zeta_{qmax} \approx \frac{1}{2\sqrt{2HK_S}} \frac{w_0 E'_q \sin(\delta_0/2)}{2} k_q. \quad (34)$$

Equation (33) shows that the optimal placement of STATCOM without BES is located between SG and infinite bus such that $X_{T2} = \frac{1}{2}(X'_d + X_T)$, i.e., the electrical mid-point of the transmission line. This optimal placement is consistent with the conventional optimal placement, where the power transfer capability and transient stability enhancement is used as the measure for different locations of STATCOM [30].

5.3. Comparison between STATCOM with and Without BES

Normally, $X_T > X'_d$, thus D_{dmax} in (22) is

$$\zeta_{dmax} > \frac{1}{2\sqrt{2HK_S}} \frac{w_0 E'_q}{2} k_d. \quad (35)$$

As $\sin(\delta_0/2) < 1$, ζ_{qmax} in (34) is

$$\zeta_{qmax} < \frac{1}{2\sqrt{2HK_S}} \frac{w_0 E'_q}{2} k_q. \quad (36)$$

Combining (35) and (36), we find ζ_{dmax} is larger than ζ_{qmax} when $k_d = k_q$. This means that STATCOM with BES is more capable of improving SG's damping than STATCOM without BES.

6. Case Study

In this section, various simulations are carried out to verify the damping control strategy in Figure 4 as well as validate previous analytical results including

1. Due to the installment of STATCOM, the electrical power of SG is deviated. The deviated value (ΔP_e) is not equal to STATCOM's active power (P).
2. In order to maximum increase SG's damping, the optimal placement of STATCOM with BES is located at the terminal of SG, while for STATCOM without BES it should be placed at the electrical mid-point of transmission line.

The tested systems are implemented in MATLAB, and the case studies are carried out in phasor mode.

6.1. Kundur's SMIB System

Figure 5 shows the diagram of the kundur's SMIB. In this test system, $X'_d = 0.15$ pu, and the other system parameters are in [33]. The initial electrical power and reactive power of SG are $P_e = 0.9$ pu, $Q_e = 0.3$ pu. The initial infinite bus voltage $E_B = 0.995 \angle 0^\circ$ pu, and the initial internal voltage of SG $E'_q = 1.123 \angle 49.92^\circ$ pu. In the simulation, the mechanical power of SG is kept unchanged and the SG is initially working in the steady state. According to the analysis form [33], when SG's damping coefficient $D = 0$, the damping ratio $\xi = 0$ and the damped natural frequency $w_d = 1.0165$ Hz. When $D = 10$, $\xi = 0.112$ and $w_d = 1.0101$ Hz.

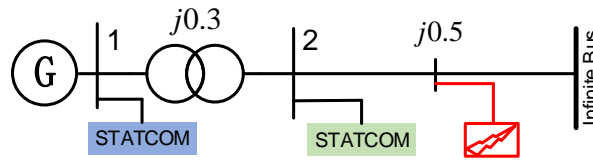


Figure 5. Kundur's SMIB system.

Firstly, the damping coefficient of SG is set as $D = 10$ and the SG is equipped with a STATCOM installed at its terminal. The active and reactive power of STATCOM are all set as zero, and step to $Q = -0.1$ pu and $P = 0.1$ pu, at $t = 1.0$ s and $t = 10.0$ s respectively. The curve of SG's deviated power ΔP_e is presented in Figure 6. As can be seen, when the active power of STATCOM is changed to $P = -0.1$ pu at $t = 1.0$ s, the electrical power of SG is also changed, and the deviated value $\Delta P_e \neq P$. Meanwhile, when the reactive power of STATCOM is changed to $Q = 0.1$ pu at $t = 10.0$ s, ΔP_e is also changed even though P is kept unchanged, and ΔP_e is not equal to P as well. This verifies that the transient active power interaction between SG and STATCOM is: $\Delta P_e \neq P$.

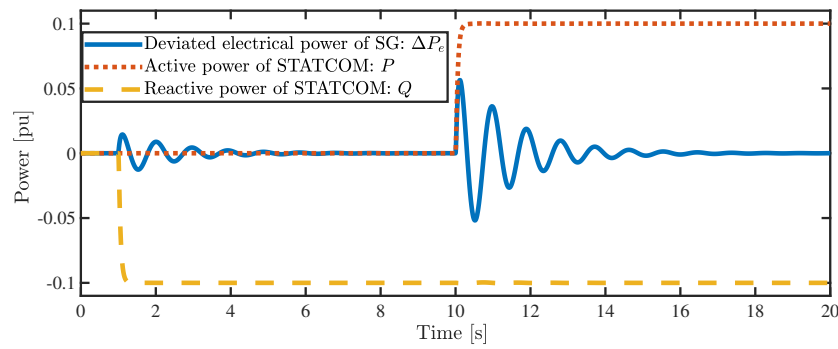


Figure 6. The SMIB system: SG's deviated electrical power ΔP_e when STATCOM's P or Q is changed.

Secondly, the damping coefficient of SG is set as $D = 0$ to emphasize the results. In this case, a one-cycle three-phase fault is applied, as indicated in Figure 5. The washout block time constant is $T_w = 10$ s. The control parameters for STATCOM with/without BES are set with the same value, i.e., $k_d = k_q = 50$. The STATCOM with and without BES are employed at the terminal of SG or Bus-2, shown in Figure 5. The time constant in (2) are set as $\tau = 5$ ms for both STATCOM with and without BES.

Figure 7 shows the results of this system with STATCOM with/without BES at different locations. The rotor angle is increasing when the fault is applied at $t = 1.0$ (seen from Figure 7a). After the fault is cleared, the system presents different behaviors under different scenarios. It should be mentioned that, at Bus-2, X_{T2} is approximately equal to $\frac{1}{2}(X'_d + X_T)$. Thus, Bus-2 should be the optimal location for STATCOM without BES according to (33).

When there is no STATCOM deployed, the rotor angle oscillation cannot be damped as SG has no damping with $D = 0$. When there is a STATCOM without BES employed at the terminal of SG, the oscillation is damped although the active power of STATCOM is kept at zero during the whole post-fault phase (shown in Figure 7b). This shows that STATCOM without BES is capable of providing damping to SG although it cannot provide active power. When the STATCOM without BES is employed at bus-2 (i.e., the optimal location), the oscillation damping is slightly improved compared with the location of SG terminal. This validates the correctness for the optimal placement for STATCOM without BES. For STATCOM with BES, we observed that the performance of the location of SG terminal is better than that of bus-2. This proves that the optimal placement for STATCOM with BES to improve system damping is at the terminal of SG. Meanwhile, the performance of STATCOM with BES is better than STATCOM without BES, which verifies that STATCOM with BES is more capable of improving SG's damping. This is because that STATCOM with BES is able to generate active power to the system (shown in Figure 7b), and thus has more ability to improve system's damping performance.

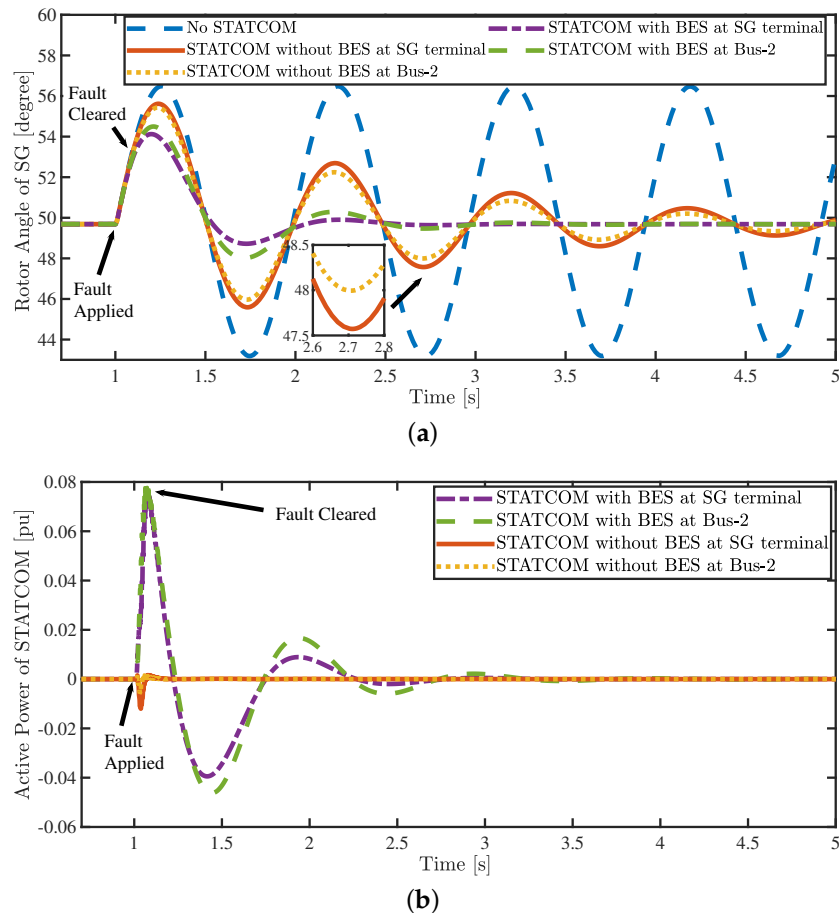


Figure 7. The SMIB system with SATCOM with/without BES at different locations. (a) Rotor angle of synchronous generator (SG); (b) Active power of STATCOM.

Table 1 further compares the overshoot of this system with STATCOM with/without BES under different locations. When there is no STATCOM installed, the overshoot of rotor angle is 6.56. When STATCOM without BES is placed at SG terminal, the overshoot is 5.69, and reduced overshoot with respect to the case of no STATCOM is 13.26%. When the same STATCOM without BES is placed at bus-2 (the electrical mid-point of transmission line), the overshoot is reduced to 5.51. This shows that the optimal location for STATCOM without BES is at the mid-point of transmission line. However, for STATCOM with BES, we notice that the oscillation is damped with the smallest overshoot when it is located at SG terminal. These results further validate the optimal placement of STATCOM with and without BES. When both STATCOM with and without BES are installed at the optimal location, the reduced overshoot of STATCOM with BES (35.98%) is larger than that of STATCOM without BES (16.01%). This observation validates that STATCOM with BES is more capable of increasing the damping of power system.

Table 1. The damping performance of SMIB with STATCOM with/without BES at different locations.

Case		Overshoot $\delta_{max} - \delta_0$ (Degree)	Reduced Overshoot (Degree)
No STATCOM		6.56	
STATCOM without BES	at SG Terminal	5.69	13.26%
	at Bus-2	5.51	16.01%
STATCOM with BES	at Bus-2	4.58	30.18%
	at SG Terminal	4.20	35.98%

6.2. The 2-Area 4-Generator System

The diagram of this system is shown in Figure 8. This test system is a multimachine power system with two areas, four generators, two loads, 12 buses and is suggested in [42] for testing the analysis and control of power system inter-area oscillations. In the simulation model, the SGs are using the subtransient reactance generator model and each of them is carried with an automatic voltage regulator, a DC exciter and a PSS. Thus, this simulation model is more detailed and realistic than our previous analytical model (i.e., SMIB model). The system parameters, such as the generator data, transmission line data, load data, can be seen in [33]. In this case study, G_1 is equipped with a STATCOM with/without BES to increase its damping, and it is placed at the terminal or at the transformer. The control parameters of STATCOM are set as $T_w = 10$ s, and the time constant in (2) are all set as $\tau = 5$ ms.

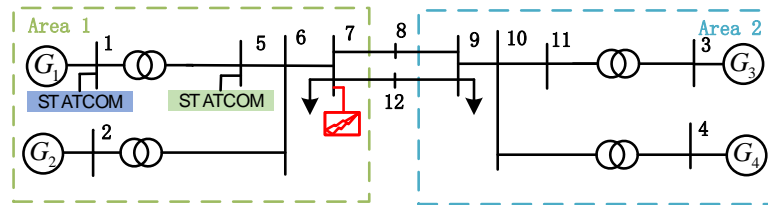


Figure 8. The two-area four-generator system.

In the first test, the mechanical power of G_1 is kept unchanged in order to show that $\Delta P_e \neq P$. The initial reactive and active power of STATCOM are all zero and step to $Q = 0.1$ pu and $P = -0.1$ pu, at $t = 1.0$ s and $t = 10.0$ s respectively. As can be seen from Figure 9, the deviated electrical power of G_1 is 0 before $t = 1.0$ s when P and Q are both unchanged. When the active power of STATCOM is stepped up to $P = 0.1$ pu at $t = 1.0$ s, the electrical power of SG is deviated ($\Delta P_e \neq 0$) and the deviated value $\Delta P_e \neq P$. When the reactive power of STATCOM is stepped down to $Q = -0.1$ pu at $t = 10.0$ s, ΔP_e is also changed even though P is kept unchanged, and the deviated value $\Delta P_e \neq P$.

In the second test, a six-cycle three-phase fault is happened at Bus-7 at $t = 1.0$ s (shown in Figure 8). As can be seen from Figure 10, when the fault is happened at $t = 1.0$ s, the rotor angle of $\delta_1 - \delta_4$ is increasing due to the loss of load at Bus-7. When G_1 is equipped with a STATCOM without BES, the system's oscillation damping performance is improved with shorter transient time and smaller overshoot, shown in Figure 10a. Meanwhile, in the location of SG transformer, the system damps the oscillation faster than the location of SG terminal. When the STATCOM is equipped with a BES, the damping performance of the location of SG terminal is better than the location of SG transformer, shown in Figure 10b. This verifies that the optimal location for STATCOM with BES is at the terminal of SG.

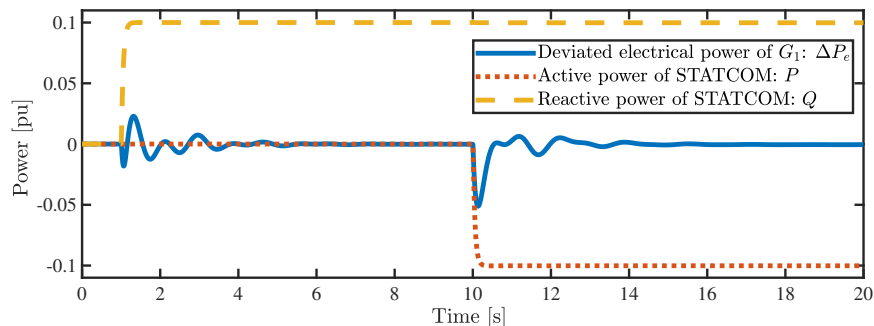


Figure 9. The two-area four-generator system: G_1 's deviated electrical power ΔP_e when STATCOM's P or Q is changed.

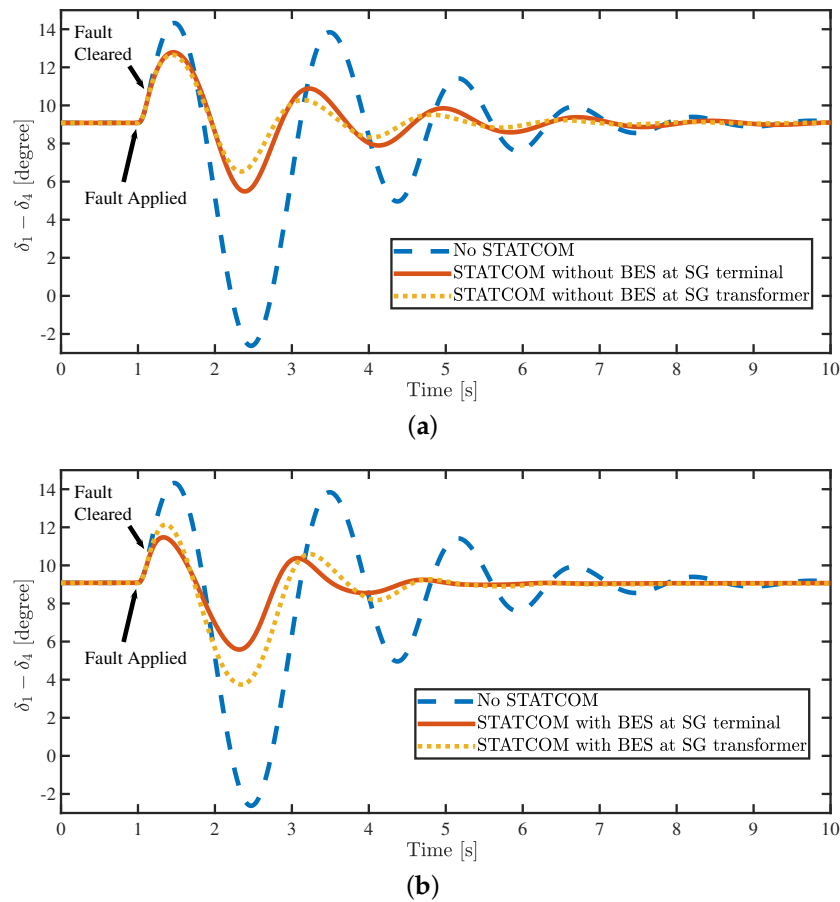


Figure 10. Optimal location of STATCOM in the two-area four-generator system. (a) Without BES; (b) With BES.

Table 2 gives the overshoot of this test system with SATCOM under different scenarios. When STATCOM without BES is placed at SG transformer, the overshoot is smaller than that of the SG terminal. However, for STATCOM with BES, the location SG terminal damps the oscillation with overshoot smaller than that of the SG transformer. These results further validate the optimal placement of STATCOM with and without BES.

Table 2. The damping performance of the two-area four-generator system with STATCOM with/without BES at different locations.

Case		Overshoot $\{\delta_1 - \delta_4\}_{max} - \{\delta_1 - \delta_4\}_0$ (Degree)	Reduced Overshoot (Degree)
No STATCOM		5.25	
STATCOM without BES	at SG Terminal	3.71	29.33%
	at SG Transformer	3.58	31.81%
STATCOM with BES	at SG Transformer	3.06	41.71%
	at SG Terminal	2.39	54.48%

A further small-signal stability analysis of STATCOM with BES (installed at the optimal location, i.e., the terminal of SG) under different k_d is shown in Figure 11a. When there is no STATCOM installed, the system's dominant eigenvalues are indicated by the blue dots in Figure 11a. When installed with a STATCOM with BES, the system's dominant eigenvalues are all on the left side of no STATCOM, indicating that the system's damping is increasing. Meanwhile, with k_d increasing from 5 to 60, the dominant eigenvalues of the system are gradually moving leftward (marked by the black arrows),

indicating that the system's damping is increasing. The above observation verifies the previous analytical results of the influence of STATCOM on SG (i.e., Equation (8)). Figure 11b compares the proposed damping controller with conventional $P_{ref} = k\Delta w$ type damper [43] under the same gain parameter. As can be seen from the black arrow, the oscillation of proposed strategy is less than that of conventional method, indicating the superiority of proposed strategy.

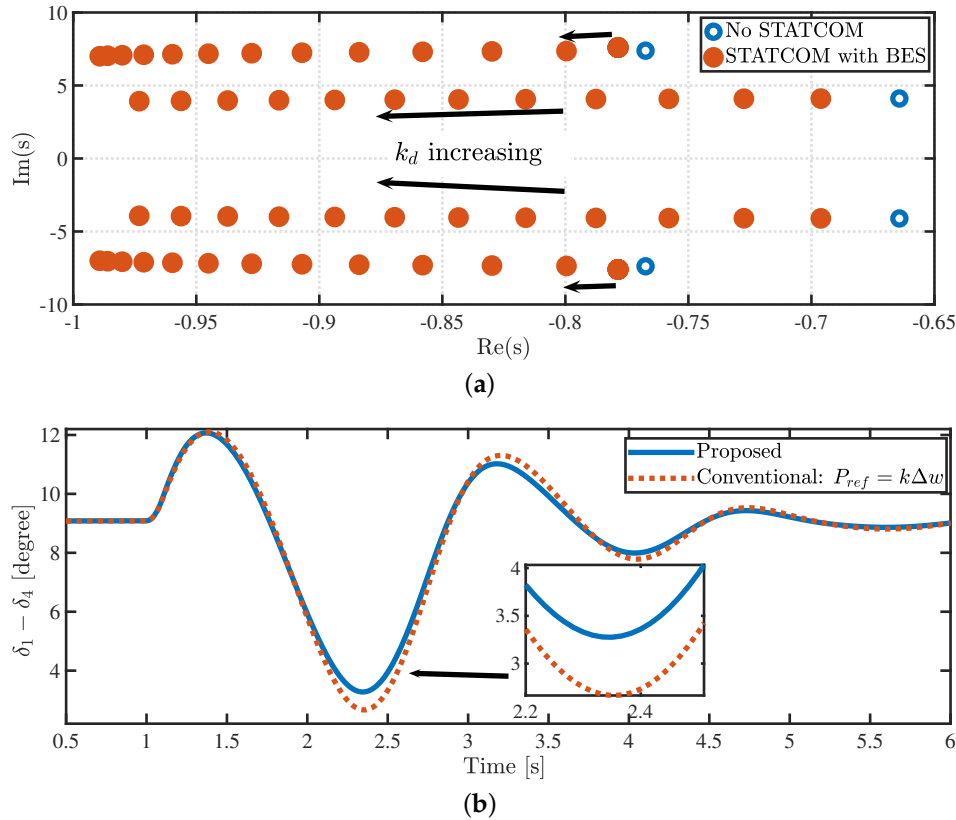


Figure 11. Results of the two-area four-generator system with STATCOM with BES. (a) Dominant eigenvalues of this system with k_d increasing; (b) Comparison with $P_{ref} = k\Delta w$ type damper.

6.3. The Australian 14-Generator Equivalent System

The previous analytical results are further validated on a five-area large power system. This test system has 14 generators, 59 buses and 29 loads, and the oscillation modes include both local and inter-area. In the simulation model, each SG is deployed with a turbine governor and a multi-band PSS with parameters tuned from [44]. The system parameters and the used simulation model can be downloaded from [44]. Besides, each generator is equipped with a STATCOM with/without BES to increase its damping, placing at the terminal or transformer. To activate the local and inter-area oscillations, a five-cycle three-phase fault is applied at the terminal of G_{101} at $t = 10$ s, shown in Figure 12.

Figure 13a depicts the trajectory of the rotor speed of G_{101} in the case of no STSTCOM and STSTCOM without BES. As can be seen, the system's oscillation is poorly damped when no STATCOM is employed. When the STATCOM without BES is installed at SG terminal with $k_q = 5$, the oscillation is damped with much smaller fluctuations. Meanwhile, in the location of SG transformer, the oscillation is damped with slightly less fluctuations than that of SG transformer (indicated by the black arrow in Figure 13a). When k_q is increased from 5 to 25, the oscillation is mitigated with further smaller overshoot and the stabilize time is reduced to at $t = 18$ s.

Figure 13b presents the results of this system in the case of STATCOM with BES. When the control parameter is set as $k_d = 25$, the system is stabilized at around $t = 14$ s, which is smaller than that

of STATCOM without BES with the same gain parameter. This shows that STATCOM with BES is more capable of increasing system's damping. When STATCOM with BES is installed at SG terminal, the damping performance is the best, i.e., with the smallest overshoot and shortest transient time. Moreover, the damping performance is increased with k_d increasing from 25 to 50. The above results further verified previous analysis and the efficiency of proposed control strategy.

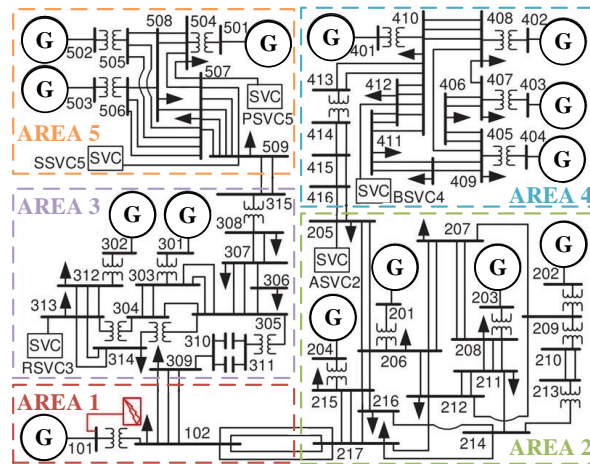


Figure 12. Australian 14-generator equivalent system.

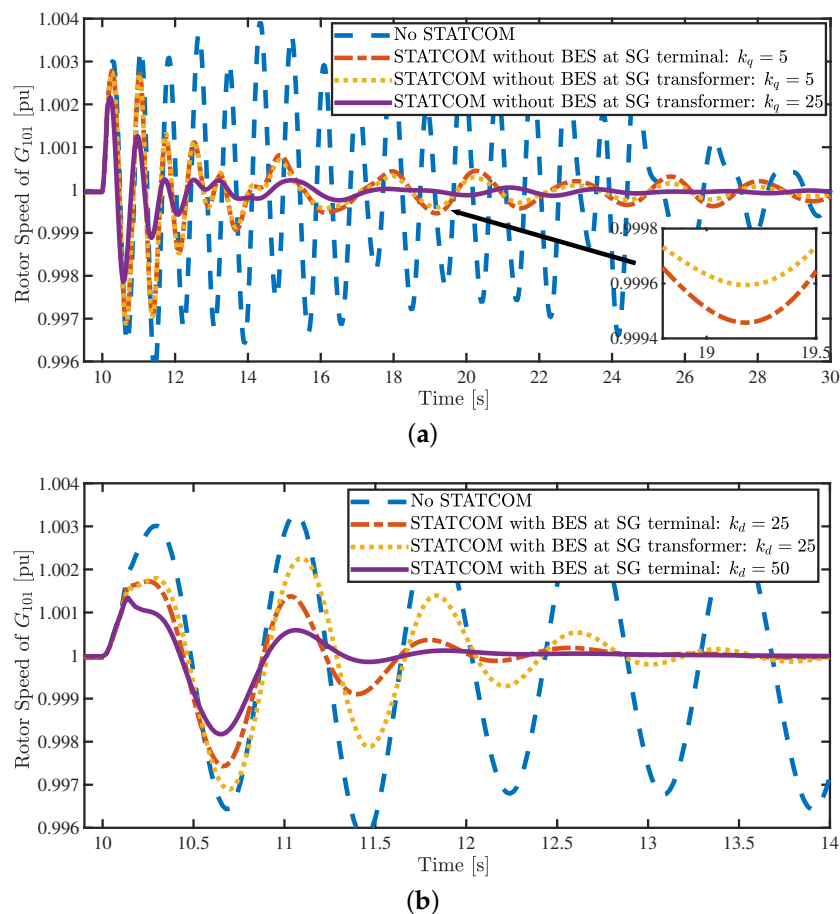


Figure 13. The Australian 14-generator equivalent system with STATCOM. (a) Without BES; (b) With BES.

A further study of the dominant eigenvalues of this system with STATCOM with BES (installed at the optimal location, i.e., the terminal of SG) is shown in Figure 14. As can be seen, when there is no STATCOM installed, the system's damping ratio is only $\zeta = 0.97\%$ (indicated by the blue arrows).

When installed with STATCOM with BES, the system's rightmost eigenvalue (indicated by the arrows) is moving leftward, indicating that the system's damping ratio is also increased. Meanwhile, with k_d increasing from 10 to 40, the system's damping ratio is increased from $\xi = 0.97\%$ to $\xi = 22.35\%$. This further validates the correctness of Equation (8).

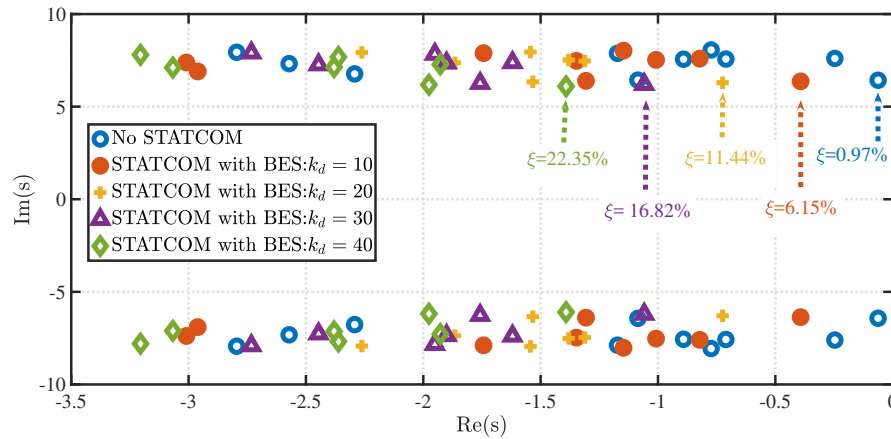


Figure 14. Dominant eigenvalues of the Australian 14-generator equivalent system with STATCOM with k_d increasing.

7. Conclusions

In this paper, the transient interaction between the active power of STATCOM with/without BES and the transient electrical power of SG is investigated. Theoretical results have shown that the deviated electrical power of SG is not equal to the active power of STATCOM with/without BES. Instead, it is determined by STATCOM's active and reactive current, STATCOM's placement, and SG's internal electrical states. Based on this, a new strategy is proposed to control STATCOM's current for improving SG's damping and thus enhancing system's damping performance. Optimal placement has also been investigated for both STATCOM with and without BES with SG's increased damping as measure. The results have shown that the optimal location for STATCOM without BES is at the electrical mid-point of the transmission line, while it is located at the terminal of SG for STATCOM with BES. Comparison between STATCOM with and without BES has shown that STATCOM with BES is more capable in increasing the damping of SG. Case studies on both kundur's SMIB system and two benchmark power systems have verified the efficiency of proposed strategy and above results.

Author Contributions: In this work, G.T. is involved in data curation, formal analysis, methodology, validation and draft writing and revision. J.X. and Y.L. provided supervision during the whole process.

Funding: This work is supported by the National Key R&D Program of China (2018YFB0904800), the National Natural Science Foundation of China (61573314, 61773339), the Technology Projects of State Grid Corporation of China (52094017000W) and the Research Project of the State Key Laboratory of Industrial Control Technology (ICT1906).

Acknowledgments: The authors would like to thank the anonymous reviewers for their valuable comments on the previous versions of this paper.

Conflicts of Interest: The authors declare no conflicts of interest.

References

1. Kundur, P.; Paserba, J.; Ajarapu, V.; Andersson, G.; Bose, A.; Canizares, C.; Hatziargyriou, N.; Hill, D.; Stankovic, A.; Taylor, C.; et al. Definition and classification of power system stability. *IEEE Trans. Power Syst.* **2004**, *19*, 1387–1401.
2. Pourbeik, P.; Kundur, P.; Taylor, C. The anatomy of a power grid blackout—Root causes and dynamics of recent major blackouts. *IEEE Power Energy Mag.* **2006**, *4*, 22–29. [[CrossRef](#)]

3. Andersson, G.; Donalek, P.; Farmer, R.; Hatziargyriou, N.; Kamwa, I.; Kundur, P.; Martins, N.; Paserba, J.; Pourbeik, P.; Sanchez-Gasca, J.; et al. Causes of the 2003 major grid blackouts in North America and Europe, and recommended means to improve system dynamic performance. *IEEE Trans. Power Syst.* **2005**, *20*, 1922–1928. [\[CrossRef\]](#)
4. Farahani, M. A multi-objective power system stabilizer. *IEEE Trans. Power Syst.* **2013**, *28*, 2700–2707. [\[CrossRef\]](#)
5. De Sousa Neto, C.M.; Costa, F.B.; de Araujo Ribeiro, R.L.; Barreto, R.L.; de Oliveira Alves Rocha, T. Wavelet-based power system stabilizer. *IEEE Trans. Ind. Electron.* **2015**, *62*, 7360–7369. [\[CrossRef\]](#)
6. Tu, G.; Li, Y.; Xiang, J.; Ma, J. Distributed Power System Stabilizer for Multimachine Power Systems. *IET Gener. Transm. Distrib.* **2019**, *13*, 603–612. [\[CrossRef\]](#)
7. Wang, Y.; Meng, J.; Zhang, X.; Xu, L. Control of PMSG-Based Wind Turbines for System Inertial Response and Power Oscillation Damping. *IEEE Trans. Sustain. Energy* **2015**, *6*, 565–574. [\[CrossRef\]](#)
8. Pipelzadeh, Y.; Chaudhuri, N.R.; Chaudhuri, B.; Green, T.C. Coordinated control of offshore wind farm and onshore HVDC converter for effective power oscillation damping. *IEEE Trans. Power Syst.* **2017**, *32*, 1860–1872. [\[CrossRef\]](#)
9. Zhou, L.; Yu, X.; Li, B.; Zheng, C.; Liu, J.; Liu, Q.; Guo, K. Damping inter-area oscillations with large-scale pv plant by modified multiple-model adaptive control strategy. *IEEE Trans. Sustain. Energy* **2017**, *8*, 1629–1636. [\[CrossRef\]](#)
10. Varma, R.K.; Akbari Kelishadi, M. Simultaneous Fast Frequency Control and Power Oscillation Damping by Utilizing PV Solar System as PV-STATCOM. *IEEE Trans. Sustain. Energy* **2019**. [\[CrossRef\]](#)
11. Del Rosso, A.D.; Canizares, C.A.; Dona, V.M. A study of TCSC controller design for power system stability improvement. *IEEE Trans. Power Syst.* **2003**, *18*, 1487–1496. [\[CrossRef\]](#)
12. Zhao, Q.; Jiang, J. Robust SVC controller design for improving power system damping. *IEEE Trans. Power Syst.* **1995**, *10*, 1927–1932. [\[CrossRef\]](#)
13. Patil, K.; Senthil, J.; Jiang, J.; Mathur, R. Application of STATCOM for damping torsional oscillations in series compensated AC systems. *IEEE Trans. Energy Convers.* **1998**, *13*, 237–243. [\[CrossRef\]](#)
14. Abido, M. Analysis and assessment of STATCOM-based damping stabilizers for power system stability enhancement. *Electr. Power Sys. Res.* **2005**, *73*, 177–185. [\[CrossRef\]](#)
15. Liu, C.H.; Hsu, Y.Y. Design of a self-tuning pi controller for a STATCOM using particle swarm optimization. *IEEE Trans. Ind. Electron.* **2010**, *57*, 702–715.
16. Rao, P.; Crow, M.; Yang, Z. STATCOM control for power system voltage control applications. *IEEE Trans. Power Del.* **2000**, *15*, 1311–1317. [\[CrossRef\]](#)
17. Abido, M.A. Design of PSS and STATCOM-based damping stabilizers using genetic algorithms. In Proceedings of the IEEE Power & Engineering Society General Meeting, Montreal, QC, Canada, 18–22 June 2006.
18. Mithulananthan, N.; Canizares, C.A.; Reeve, J.; Rogers, G.J. Comparison of PSS, SVC, and STATCOM controllers for damping power system oscillations. *IEEE Trans. Power Syst.* **2003**, *18*, 786–792. [\[CrossRef\]](#)
19. Wen, Y.; Guo, C.; Pandžić, H.; Kirschen, D.S. Enhanced security-constrained unit commitment with emerging utility-scale energy storage. *IEEE Trans. Power Syst.* **2016**, *31*, 652–662. [\[CrossRef\]](#)
20. Nguyen, C.K.; Nguyen, T.T.; Yoo, H.J.; Kim, H.M. Consensus-based SOC balancing of battery energy storage systems in wind farm. *Energies* **2018**, *11*, 3507. [\[CrossRef\]](#)
21. Lei, M.; Yang, Z.; Wang, Y.; Xu, H.; Meng, L.; Vasquez, J.C.; Guerrero, J.M. An MPC-Based ESS Control Method for PV Power Smoothing Applications. *IEEE Trans. Power Electron.* **2018**, *33*, 2136–2144. [\[CrossRef\]](#)
22. Moon, H.J.; Kim, Y.J.; Chang, J.W.; Moon, S.I. Decentralised active power control strategy for real-time power balance in an isolated microgrid with an energy storage system and diesel generators. *Energies* **2019**, *12*, 511. [\[CrossRef\]](#)
23. Farraj, A.; Hammad, E.; Kundur, D. A cyber-enabled stabilizing control scheme for resilient smart grid systems. *IEEE Trans. Smart Grid* **2016**, *7*, 1856–1865. [\[CrossRef\]](#)
24. Trevizan, R.D.; Ayar, M.; Bretas, A.S.; Obuz, S. Cooperative Control of Energy Storage for Transient Stability Enhancement. In Proceedings of the IEEE Power & Energy Society General Meeting (PESGM), Portland, OR, USA, 5–9 August 2018; pp. 1–5.
25. Farraj, A.; Hammad, E.; Kundur, D. On the use of energy storage systems and linear feedback optimal control for transient stability. *IEEE Trans. Ind. Informat.* **2017**, *13*, 1575–1585. [\[CrossRef\]](#)

26. Ayar, M.; Obuz, S.; Trevizan, R.; Bretas, A.; Latchman, H. A distributed control approach for enhancing smart grid transient stability and resilience. *IEEE Trans. Smart Grid* **2017**, *8*, 3035–3044. [\[CrossRef\]](#)
27. Farraj, A.; Hammad, E.; Kundur, D. On the impact of cyber attacks on data integrity in storage-based transient stability control. *IEEE Trans. Ind. Informat.* **2017**, *13*, 3322–3333. [\[CrossRef\]](#)
28. Lucia, W.; Gheitsi, K.; Bagherzadeh, M. A Low Computationally Demanding Model Predictive Control Strategy for Robust Transient Stability in Smart Grid. In Proceedings of the IEEE Conference on Decision and Control (CDC), Miami Beach, FL, USA, 17–19 December 2018; pp. 6013–6018.
29. Farraj, A.; Hammad, E.; Kundur, D. A Storage-Based Multiagent Regulation Framework for Smart Grid Resilience. *IEEE Trans. Ind. Informat.* **2018**, *14*, 3859–3869. [\[CrossRef\]](#)
30. Shahnia, F.; Rajakaruna, S.; Ghosh, A. *Static Compensators (STATCOMs) in Power Systems*; Springer: Singapore, 2015.
31. Lu, Q.; Sun, Y.; Mei, S. *Nonlinear Control Systems and Power System Dynamics*; Springer: New York, NY, USA, 2013; Volume 10.
32. Demello, F.P.; Concordia, C. Concepts of synchronous machine stability as affected by excitation control. *IEEE Trans. Power Appl. Syst.* **1969**, *88*, 316–329. [\[CrossRef\]](#)
33. Kundur, P.; Balu, N.J.; Lauby, M.G. *Power System Stability and Control*; McGraw-Hill: New York, NY, USA, 1994; Volume 7.
34. Grigsby, L.L. *Electric Power Generation, Transmission, and Distribution*; CRC Press: Boca Raton, FL, USA, 2007.
35. Kazmierkowski, M.P.; Malesani, L. Current control techniques for three-phase voltage-source PWM converters: A survey. *IEEE Trans. Ind. Electron.* **1998**, *45*, 691–703. [\[CrossRef\]](#)
36. Kanchanaharuthai, A.; Chankong, V.; Loparo, K.A. Transient Stability and Voltage Regulation in Multimachine Power Systems Vis-à-Vis STATCOM and Battery Energy Storage. *IEEE Trans. Power Syst.* **2015**, *30*, 2404–2416. [\[CrossRef\]](#)
37. Yazdani, A.; Iravani, R. *Voltage-Sourced Converters in Power Systems*; Wiley Online Library: Hoboken, NJ, USA, 2010; Volume 34.
38. Yu, Y.N. *Electric Power System Dynamics*; Academic Press: New York, USA, 1983; Volume 2.
39. Sui, X.; Tang, Y.; He, H.; Wen, J. Energy-storage-based low-frequency oscillation damping control using particle swarm optimization and heuristic dynamic programming. *IEEE Trans. Power Syst.* **2014**, *29*, 2539–2548. [\[CrossRef\]](#)
40. Shi, L.; Lee, K.Y.; Wu, F. Robust ESS-based stabilizer design for damping inter-area oscillations in multimachine power systems. *IEEE Trans. Power Syst.* **2016**, *31*, 1395–1406. [\[CrossRef\]](#)
41. Kumar, A. Power System Stabilizers Design for Multimachine Power Systems Using Local Measurements. *IEEE Trans. Power Syst.* **2016**, *31*, 2163–2171. [\[CrossRef\]](#)
42. Canizares, C.; others. Benchmark models for the analysis and control of small-signal oscillatory dynamics in power systems. *IEEE Trans. Power Syst.* **2017**, *32*, 715–722. [\[CrossRef\]](#)
43. Zhu, Y.; Liu, C.; Sun, K.; Shi, D.; Wang, Z. Optimization of Battery Energy Storage to Improve Power System Oscillation Damping. *IEEE Trans. Sustain. Energy* **2019**, *10*, 1015–1024. [\[CrossRef\]](#)
44. Moeini, A.; Kamwa, I.; Brunelle, P.; Sybille, G. Open data IEEE test systems implemented in SimPowerSystems for education and research in power grid dynamics and control. In Proceedings of the 50th International Universities Power Engineering Conference (UPEC), Stoke on Trent, UK, 1–4 September 2015; pp. 1–6.

